Distribution Statement

Distribution A: Public Release.

The views presented here are those of the author and are not to be construed as official or reflecting the views of the Uniformed Services University of the Health Sciences, the Department of Defense or the U.S. Government.

Targeted Endodontic Microsurgery: Implications of the Greater Palatine Artery

Bracken G. Smith, Allen M. Pratt, Jarom Ray

Research is complete.

[redacted], 17 June 2020

Allen M. Pratt, D.M.D
Program Director

[redacted], 17 June 2020

Jarom J. Ray, D.D.S
Training Officer

[redacted], 17 Jun 2020

Jay D. Graver, D.M.D., M.S.
Dean, Air Force Postgraduate Dental School

17 June 2020

The author hereby certifies that the use of any copyrighted material in the thesis manuscript entitled:

Targeted Endodontic Microsurgery: Implications of the Greater Palatine Artery

is appropriately acknowledged, beyond brief excerpts and is with the permission of the copy owner.

_____

Signature

Bracken G. Smith, Maj, USAF, DC

Printed Name

Endodontic Residency, AFPDS JBSA-Lackland

Program and Program Location

Uniformed Services University

Targeted Endodontic Microsurgery: Implications of the Greater Palatine Artery

Smith, Bracken G, DMD; Pratt, Allen M, DMD; Anderson, Julie A, DMD; Ray, Jarom J, DDS

ABSTRACT

Introduction: Targeted Endodontic Microsurgery (TEMS) combines trephine burs and 3D-printed guides to make flapless maxillary palatal root-end surgery possible. This study assessed the location of the greater palatine artery (GPA), the relationship of the GPA to maxillary molar root-ends, and the feasibility of flapless palatal-approach TEMS.
Methods: Three endodontists analyzed 250 CBCT images of maxillary molars for: 1) transition morphology between the hard palate and the alveolar process adjacent to first and second molars as an indication of the most likely location of the GPA, 2) the superior-inferior relationship between the GPA and root-ends, and 3) the feasibility of palatal-approach TEMS.
Results: Palatal transition morphology (PTM) included 20% Spine, 72% Bridge, and 8% Smooth. GPA location as related to palatal root-ends was classified as 34% superior, 40% adjacent, and 21% inferior. Five percent of classifications were undefined. TEMS was deemed feasible for 47% of maxillary first molars, 52% of second molars, and was significantly more feasible with GPAs superior to palatal root-ends. Reasons for infeasibility included GPA proximity and unfavorable resection angle or level. Maxillary first molar palatal roots were 11.13 $\pm$ 2.68 mm from the greater palatine foramen (GPF) and 2.37 $\pm$ 1.46 mm from the GPA. Second molar palatal roots were 4.94 $\pm$ 2.55 mm from the GPF and 2.53 $\pm$ 1.77 mm from the GPA.
Conclusions: PTM and GPA position adjacent to maxillary molars, as manifested in CBCT coronal views, suggested maxillary palatal root TEMS could be accomplished with a 2 mm safety margin in 47% of first molars and 52% of second molars. Historical paradigms that do not consider flapless palatal surgical approaches may need to be revised.

KEY WORDS

Targeted Endodontic Microsurgery; greater palatine artery; maxillary molar; cone-beam computed tomography; 3D-printed; trephine; surgical guide

SIGNIFICANCE

Flapless palatal-approach Targeted Endodontic Microsurgery may be a viable option for nearly half of maxillary first and second molars. Palatal transition morphology in coronal-section cone beam computed tomography can aid in anticipating greater palatine artery position during surgical evaluation and treatment planning.

INTRODUCTION

Maxillary molar palatal surgical approaches are rare in part owing to the proximity of root apices to the greater palatine foramen (GPF) and greater palatine artery (GPA). Targeted Endodontic Microsurgery (TEMS) uses three-dimensional (3D) printed surgical guides with trephine burs for flapless palatal-approach osteotomy, resection and fill of maxillary first and second molar palatal roots (1). TEMS uses a biopsy punch in a rotary handpiece and careful dissection to remove palatal masticatory mucosa which is set aside for later use. Next a cylindrical trephine bur rotating within a surgical guide produces a precise osteotomy and resection with

depth, diameter, and angulation exquisitely prescribed within implant planning software (1-3). TEMS produces a cylindrical core biopsy sample containing bone, root, and soft tissue lesion that is removed prior to root end preparation and fill. Finally, palatal masticatory mucosa is replaced and sutured over the crypt to act as a surgical dressing during healing (1). Along with understanding principles of digital design and 3D printing for guide fabrication (2,4), the technique requires a sound appreciation of palatal anatomy for safe and effective diagnosis and treatment. (1,5,6).

Because the GPA can be the source of significant surgical and post-surgical complications, an appreciation of its anatomical location and size is essential. The maxillary artery gives off the descending palatine artery which becomes the GPA as it exits the GPF at a site described as medial to the third molar, about 3 mm from the osseous crest and 18-20 mm from the occlusal plane (7-12). The maxillary division of the trigeminal nerve gives off the greater palatine nerve (GPN) which passes through the GPF to course anteriorly in superomedial association with the GPA (7,13,14). The GPF is described as a 4.1 x 2.8 mm anteroposterior elongated opening that is often contiguous with an osseous groove that courses anteriorly at the junction of the alveolus and the hard palate, partially enwrapping the GPA (7,10,13-16). The inferior border of the GPA lies 12-14 mm superior to the cemento-enamel-junction (CEJ) of maxillary molars (16-20). The GPA diameter averages 2.65 mm at the GPF and gradually decreases to 0.8 mm at the first premolar area (15-16,21). Implant placement literature calls for a 2 mm safety margin between vital structures and a prospective guided osteotomy (22). This recommendation is pertinent to safe palatal-approach TEMS; however, dimensional averages regarding GPA position from cadavers, *ex vivo* human skulls, and CBCT studies cannot arbitrarily be applied to individual patients (8,13-20). Rather, clinicians must consider the patient's distinctive anatomic presentation during diagnosis and treatment planning.

The confluence of the hard palate and the alveolus makes up an anatomic "transition" area with variable *palatal transition morphology* (PTM) (Fig. 1) that is important for understanding the most likely position of the GPA (13-14,18). Cadaver analyses suggested a dissection-based, three-category PTM classification of *Spine* Type (with a definitive bony spine), *Bridge* Type (with a less pronounced bony prominence), or *Smooth* Type (lacking a bony prominence altogether) (14). The same PTM visible via cadaveric dissections can be assessed in live patients with CBCT (23), allowing for adaptation of the dissection-based classification to clinical scenarios. Understanding the most likely position of the GPA according to PTM, and in relation to palatal roots, will determine if TEMS is feasible with a 2 mm safety margin.

This study aimed to use CBCT coronal sections to: 1) establish a CBCT-based PTM classification to aid in GPA location for TEMS diagnosis and treatment planning; 2) classify the position of the GPA as superior, adjacent, or inferior to palatal root tips; 3) measure the distance from prospective palatal roots to the GPF and GPA and from molar CEJs to the GPA; 4) establish the relative feasibility of safely and effectively accomplishing TEMS with a 2 mm safety margin, as determined by three experienced endodontists; and 5) compare TEMS feasibility appraisals to the positional and dimensional assessments of the GPF and GPA relative to palatal roots. The null hypothesis was that, within the study's cohort of patient CBCTs, the likely location of the GPA in maxillary molar regions could be established in all cases, and that given this location in relation to palatal root tips, TEMS could be safely carried out with a 2 mm safety margin for all palatal roots of maxillary first and second molars. Furthermore, we hypothesized that *TEMS-feasible* designations would be significantly related to a more superior position of the GPA in relation to palatal root tips, as well as larger measurements between palatal roots and the GPF and GPA, and molar CEJs and the GPA.

MATERIALS AND METHODS

The 59th Medical Wing Institutional Review Board approved the study.

Calibration and Development of Classifications

Prior to experimentation, three endodontists that utilize TEMS for palatal surgery viewed a comprehensive presentation chronicling the pertinent GPA and PTM dry skull, cadaver, and CBCT-based literature (7-23) including detailed depictions of the GPF; the course, diameter, and branching patterns of the GPA; the variations in PTM; the relationship of the GPA to palatal roots; and the concept of a 2 mm safety zone.

Next authors viewed several CBCT coronal sections with disparate PTM and adapted concepts from cadaver studies (13-14) to establish a *CBCT Coronal Section PTM Classification* as follows: 1) *Spine* Type PTM with a definitive bony spine separating medial and lateral grooves, 2) *Bridge* Type PTM lacking a bony spine but containing a distinct bony groove at the confluence of the hard palate and alveolus, and 3) *Smooth* Type PTM lacking spine or bridge morphology but with a smooth arc at the confluence of the alveolus and hard palate (Fig. 1). Based upon GPA location described in cadaveric studies (13-14) the most likely location of the GPA as applied to CBCT-based bony PTM was designated to be in the lateral groove for *Spine* Type PTM or in the single groove for *Bridge* Type PTM. For *Smooth* Type PTM no definitive landmark denoted the likely position of the GPA; therefore, the GPA was designated to most likely lie tangential to and centered in the confluent arc between the hard palate and alveolus. Finally, authors defined a three-tiered *TEMS GPA Classification* designating the GPA as being *Superior, Adjacent, Inferior* or *Undefined* with respect to a horizontal line drawn parallel to the hard palate from a given maxillary molar palatal root apex (Fig. 2).

CBCT Selection

A cohort of patient CBCT scans was randomly selected for inclusion from the Air Force Postgraduate Dental School database from January 2017 to October 2018 according to the following criteria: patients $\geq$ 22 years old, maxillary first and second molars visible in coronal section, absence of artifact or distortion in the area of interest, and GPF location distal to the maxillary second molar palatal root tip. Entire left or right sides of CBCT scans were excluded if the maxillary first or second molar had significant bone loss, apical surgery, apical palatal root resorption, or had been extracted. The selected cohort included studies with 40 x 40, 60 x 60, or 80 x 80 mm fields with respective voxel sizes of 0.08, 0.125 and 0.160 mm acquired with a 3D Accuitomo 170 (J. Morita USA, Irvine, CA) at 5-7 mA, 65-90 kVp, and a 17.5 second exposure time.

Anatomical Measurements

The primary author used iDixel software (Version 2.2.0.3; J. Morita USA, Irvine, CA) to orient individual coronal sections that bisected the long axis of maxillary molar palatal roots at their apices. Circles representing the likely diameter of the GPA (2.5 mm for the second molar region; 2.35 mm for the first molar region), as adapted from the literature (15-16,21), were positioned according to the conventions applied to the *CBCT Coronal Section PTM Classification* (Fig. 3). During placement of circles, the primary author had access to the entire CBCT such that multiple views cold be utilized to identify the most likely position of the GPA. A second circle representing a 2 mm safety margin was centered over the GPA location (Fig. 3). After calibration

by oral and maxillofacial radiologists, the primary author manipulated images in axial, coronal, and sagittal views to obtain the following distance measurements: maxillary molar palatal root to the closest border of the GPF, maxillary molar palatal root to the closest border of the GPA, and maxillary molar CEJ to the inferior border of the GPA (Fig. 4). Patient age and sex were recorded.

Clinician Assessment

Evaluators individually viewed the coronal section cohort applying previously established PTM concepts to assess the following: 1) PTM Type (*Spine*, *Bridge*, or *Smooth*) (Fig. 1); 2) agreement or disagreement with the location of the GPA established by the primary author (agree or disagree); 3) TEMS Classification of GPA position as Superior, Adjacent, Inferior or Undefined (Fig. 2). Lastly, clinicians rendered a clinical opinion regarding the feasibility of carrying out TEMS with a 2 mm safety margin (yes or no). If TEMS was deemed infeasible, evaluators selected up to three reasons from the following: proximity to the GPA (violates safety margin), proximity to the sinus (potential for irretrievable root tip), unfavorable resection angle (too steep), unfavorable resection length (excessive root removal), unfavorable cortical thickness and root end "depth" (adversely affecting root-end visualization or manipulation), or other (written specification). Evaluators later repeated individual assessments of 30 randomly selected teeth from the coronal section cohort for reliability assessment. PTM type, GPA site and classification, and TEMS feasibility were determined by majority (2 of 3) agreement among evaluators.

Statistical Analyses

Statistical analyses were performed using SAS Version 9.4 (Statistical Analysis Software, Cary, NC) with significance set to $p < 0.05$. Anatomical measurements were assessed for normality with the Shapiro-Wilks test; analyzed for significant associations with patient gender, side (right or left), and tooth type using Independent t-tests; and checked for associations with patient age using Pearson correlation.

Measurements and patient demographics were analyzed for associations with PTM types, GPA classifications, and TEMS feasibility using one-way analyses of variance (ANOVA) and Tukey's post hoc tests. Associations between evaluator assessments of PTM types, GPA classifications, and TEMS feasibility, as well associations between evaluator assessments and patient side and tooth type, were analyzed for significance with Chi-Squared tests.

Evaluator agreement was measured using Fleiss's kappa for inter-rater reliability and intraclass correlation coefficients (ICC) for intra-rater reliability. Kappa values of < 0.00 were considered "poor agreement," 0.00-0.20 "slight," 0.21-0.40 "fair," 0.41-0.60 "moderate," 0.61-0.80 "substantial," and > 0.80 "almost perfect" (24). ICC values of < 0.5 were considered "poor," 0.5-0.75 "moderate," 0.75-0.90 "good," and > 0.90 "excellent" (25).

RESULTS

A total of 250 teeth including 126 maxillary first molars and 124 maxillary second molars were evaluated from 92 patient CBCT scans including 47 females (51%) and 45 males (49%). There were 115 right molars (46%) and 135 left molars (54%). The average patient age was 42 years (median 38.5; range 22-81).

Anatomical Measurements

Mean distances from maxillary molar palatal roots and CEJs to the GPF and GPA are presented in Tables 1-3. The mean distance from first molar palatal roots to the GPF (11.13 ±

2.68 mm) was significantly greater than for second molars (4.94 ± 2.55 mm; $p < 0.0001$). The mean distance from first molar CEJs to the GPA was significantly smaller (12.86 ± 2.29 mm) than for second molars (14.05 ± 2.52 mm; $p = 0.0001$). The mean CEJ to GPA distance was significantly smaller for females (12.54 ± 2.56 mm) than for males (14.33 ± 2.04 mm; $p < 0.0001$). Increased age was positively correlated with greater distance from the CEJ to the GPA ($r = 0.30$; $p < 0.0001$).

Clinician Assessment: PTM Type

PTM included 180 *Bridge* (72%), 50 *Spine* (20%), and 20 *Smooth* (8%). There were significantly more *Spine* transition types adjacent to maxillary first molars than to maxillary second molars ($p = 0.0065$). The mean age of patients demonstrating *Smooth* transition morphology (51.75 ± 15.49 years) was significantly higher than those demonstrating *Spine* morphology (41.26 ± 14.06 years) and *Bridge* morphology (40.32 ± 13.63 years; $p = 0.0025$).

Clinician Assessment: GPA Classification

At least two of three evaluators agreed with the primary author's GPA positioning for 230 teeth (92%), agreed that the position could not be reliably determined for 15 teeth (6%), but disagreed for 5 teeth (2%). TEMS Classifications relating GPA position to maxillary molar palatal root-ends included 100 adjacent (40%), 85 superior (34%), 52 inferior (21%), and 13 undetermined (5%). For the maxillary first molar, the GPA was adjacent to 49 (39%), superior to 36 (29%), and inferior to 34 (27%). For the maxillary second molar, the GPA was adjacent to 51 (41%), superior to 49 (40%), and inferior to 18 (15%). A significantly greater number of undefined GPA classifications were associated with *Smooth* PTM ($p < 0.0001$). There was no significant association between tooth type and GPA classification.

Clinician Assessment: TEMS Feasibility

TEMS was deemed feasible for 124 teeth (49.6%) including 59 maxillary first molars (47%) and 65 maxillary second molars (52%) (Fig. 5). TEMS feasibility was significantly higher for superior GPA classifications over adjacent and inferior ($p < 0.0001$), and for adjacent over inferior ($p < 0.0001$). Inferior GPA classifications were deemed infeasible significantly more than undefined classifications ($p < 0.0001$). There was no significant association between PTM and TEMS feasibility.

Evaluators indicated up to three reasons per tooth for the 126 TEMS-infeasible teeth (50.4%). Reasons for maxillary first molars included proximity to the GPA (91%), unfavorable resection angle (15%), proximity to the sinus (8%), and unfavorable resection length (5%). Reasons for maxillary second molars included proximity to the GPA (86%), unfavorable resection angle (18%), unfavorable resection length (9%), unfavorable root depth (3%), other (2% specified as removal of supporting bone and possible accessory vasculature), and proximity to the sinus (1%).

Anatomical Measurements and PTM Type

The mean distances from maxillary molar palatal roots to the GPF for *Spine* PTM (10.12 ± 3.98 mm) and for *Smooth* PTM (9.56 ± 3.46 mm) were significantly greater than that mean distance for *Bridge* PTM (7.32 ± 3.91 mm; $p < 0.0001$). The mean distance from palatal roots to the GPA for *Smooth* PTM (3.78 ± 1.41 mm) was significantly greater than the mean distance for *Spine* PTM (2.22 ± 1.62 mm) and for *Bridge* PTM (2.36 ± 1.58 mm; $p = 0.0004$). The mean distance from maxillary molar CEJs to the GPA for *Smooth* PTM (14.90 ± 2.82 mm) was

significantly greater than that mean distance for *Spine* PTM (13.05 ± 2.21 mm) and for *Bridge* PTM (13.40 ± 2.46 mm; p = 0.015).

Anatomical Measurements and GPA Classification

Mean distances from maxillary molar palatal roots to the GPF and GPA were significantly greater for superior GPA classifications (GPF 8.85 ± 3.88 mm; GPA 3.67 ± 1.68 mm) than for adjacent classifications (GPF 7.28 ± 4.21 mm, p = 0.04; GPA 1.79 ± 1.09, p < 0.0001). The mean root-to-GPA distance for undefined classifications (3.38 ± 1.33 mm) was significantly greater than for adjacent (1.79 ± 1.09 mm) and inferior classifications (1.49 ± 0.96 mm, p <0.0001). The mean molar CEJ-to-GPA distance for superior GPA classifications (15.30 ± 1.72 mm) was significantly greater than for adjacent (13.00 ± 1.89 mm) and inferior classifications (10.96 ± 2.02 mm, p <0.0001). The mean CEJ-to-GPA distance for undefined classifications (14.77 ± 2.15 mm) was significantly greater than for adjacent and inferior classifications (p < 0.0001), as well as for adjacent classifications over inferior classifications (p < 0.0001).

Anatomical Measurements and TEMS Feasibility

Mean distances from maxillary molar palatal roots to the GPF and GPA were significantly longer in cases where TEMS was deemed feasible (GPF 8.82 ± 3.74 mm and GPA 3.36 ± 1.59 mm) than in cases where TEMS was not deemed feasible (GPF 7.31 ± 4.23 mm, p = 0.003; and GPA 1.55 ± 1.04 mm, p < 0.0001). Likewise, mean distances from molar CEJs to the GPA were significantly longer in cases where TEMS was deemed feasible (14.67 ± 2.03 mm) than in cases where TEMS was not feasible (12.26 ± 2.28 mm, p < 0.0001). There were no significant differences between right and left sides for evaluator assessments or anatomical measurements.

Rater Agreement

Inter-rater agreement was “substantial” for PTM type (kappa = 0.76) and “almost perfect” for GPA classification and TEMS feasibility (kappa = 0.99 and 0.81, respectively) (24). Intra-rater reliability was “good” for transition morphology, GPA classification, and TEMS feasibility (ICC = 0.79, 0.89, and 0.86, respectively) (25).

DISCUSSION

The null hypothesis that the likely location of the GPA could be successfully identified in all coronal sections of the cohort was rejected due to a number of *Smooth* Type PTM. Furthermore, the hypothesis that palatal-root TEMS could be successfully carried out with a 2 mm safety margin for all patients in this cohort, as determined by at least two of three experienced clinicians, was rejected. Conversely, the hypothesis that TEMS-*feasible* clinician designations would be significantly related to a more superior position of the GPA in relation to palatal root tips was accepted. Finally, the hypothesis that TEMS-*feasible* clinician designations would be significantly related to a larger distance between maxillary molar palatal roots or CEJs and the GPF and GPA was accepted.

The CBCT Coronal Section PTM Classification adapted from previous cadaver-dissection studies (13-14) resulted in substantial inter-rater agreement when applied to this cohort by calibrated TEMS clinicians, suggesting a viable means of assessing patient CBCT in the clinic and for conducting future CBCT-based research. Data indicate that the TEMS GPA Classification describing the position of the GPA as superior, adjacent, or inferior to the palatal root tip may be

useful in assessment for palatal-root TEMS. Our findings corroborate measurements of the distance from the maxillary molar CEJ to the GPA described in cadaver and CBCT studies (13-20). Measurements of the distance from maxillary molar palatal roots to the GPA have not been previously reported, nor have they been related to the feasibility of palatal-approach root-end resection. As such, these data are valuable contributions to the body of endodontic surgical literature. Experienced clinicians deemed palatal-approach TEMS feasible for roughly half of maxillary molars, suggesting that historical paradigms that do not include the possibility of palatal surgical approaches may need to be revised.

Results should be interpreted in consideration of some limitations. First, the location of the GPA can only be definitively determined with dissection. We used PTM as a surrogate indicator of the most likely location of the GPA. Cadaver-based studies suggest this methodology is valid because the GPA generally follows a course indicated by osseous landmarks, when present, in the area of the first and second molars (13-14). Second, using one CBCT coronal section that passed through the apex of maxillary molar palatal roots allowed for standardization and efficiency in evaluating a large number of potential surgical sites. However, the entire patient CBCT with axial, coronal, and sagittal views is available to clinicians, possibly expanding capability to determine the position of the vessel as it courses anteriorly from the GPF. Further, it is possible that clinicians may encounter anatomic variation that does not readily conform to the PTM classification of *Spine*, *Bridge*, and *Smooth* Types, for example, in patients with two spines or two bridge prominences (Fig. 1). In such cases it is essential that clinicians use multiple CBCT sections to establish the most likely location of the GPF and GPA. Future research on clinical technique and outcomes assessment of palatal-approach TEMS is warranted.

This study identified *Spine* Type PTM for 20% of coronal sections compared to gold-standard cadaver studies that identified spine morphologies in 34-69% of PTM (14,26-27). This may be explained by relative sample size differences between this cohort and more limited cadaver studies, or by evaluators viewing only one surgically relevant area near palatal roots in this study, versus the entire posterior sextant in cadaver studies.

CONCLUSIONS

PTM as viewed in CBCT coronal sections discloses the most likely location of the GPA, allowing for appreciation of both the vertical and horizontal dimensional relationships between the GPA and maxillary molar palatal roots. Within this cohort of CBCT coronal sections, at least two of three experienced clinicians deemed TEMS (accomplished with a 2 mm safety margin) as feasible for roughly half of maxillary molars. Historical paradigms that do not consider flapless palatal surgical approaches may need to be revised.

AUTHORS

Capt Bracken G. Smith, DMD, Resident, Air Force Postgraduate Dental School and Uniformed Services University of the Health Sciences Postgraduate Dental College.

Lt Col Allen M. Pratt, DMD, Endodontics Residency Training Officer, Air Force Postgraduate Dental School and Uniformed Services University of the Health Sciences Postgraduate Dental College.

Capt Julie A. Anderson, DMD, Endodontist, Air Force Postgraduate Dental School and Hurlburt Field Dental Clinic.

Lt Col Jarom J. Ray, DDS, Endodontics Residency Program Director, Air Force Postgraduate Dental School and Uniformed Services University of the Health Sciences Postgraduate Dental College.

The views expressed are those of the authors and do not reflect the official views or policy of the Department of Defense or its Components or the Uniformed Services University of the Health Sciences.

The authors deny any conflicts of interest related to this study.

ACKNOWLEDGEMENTS

All artwork is original and was created by the primary author.

Special acknowledgments to Dr. Shawn Countryman and Dr. Hassem Geha for Oral and Maxillofacial Radiology calibration and to Dr. Jisuk Park for statistical support.

REFERENCES

1. Giacomino CM, Ray JJ, Wealleans JA. Targeted endodontic microsurgery: a novel approach to anatomically challenging scenarios using 3-dimensional-printed guides and trephine burs-a report of 3 cases. J Endod 2018;44:671-7.

2. Ray JJ, Giacomino CM, Wealleans JA, Sheridan RR. (2020). Targeted endodontic microsurgery: digital workflow options. J Endod 2020;46:863-70.

3. Hawkins TK, Wealleans JA, Pratt AM, Ray JJ. Targeted endodontic microsurgery and endodontic microsurgery: a surgical simulation comparison. Int Endod J 2020;53:715-22.

4. Anderson J, Wealleans J, Ray J. Endodontic applications of 3D printing. Int Endod J 2018;51:1005-18.

5. Lavasani SA, Tyler C, Roach SH, et al. Cone-beam computed tomography: anatomic analysis of maxillary posterior teeth-impact on endodontic microsurgery. J Endod 2016;42:890-5

6. Lee SH, Cho SY, Kim DH, Jung IY. Clinical outcomes after apical surgery on the palatal root of the maxillary first molar using a palatal approach. J Endod 2020;46:464-70.

7. Norton NS, Netter FH. Netter's Head and Neck Anatomy for Dentistry, 1st ed. Philadelphia, PA: Saunders Elsevier; 2007:343-97.

8. Tomaszewska IM, Tomaszewski KA, Kmiotek EK, et al. Anatomical landmarks for the localization of the greater palatine foramen--a study of 1200 head CTs, 150 dry skulls, systematic review of literature and meta-analysis. J Anat 2014;225:419-35.

9. Bahşi İ, Orhan M, Kervancıoğlu P, Yalçın ED. Morphometric evaluation and clinical implications of the greater palatine foramen, greater palatine canal and pterygopalatine fossa on CBCT images and review of literature. Surg Radiol Anat 2019;41:551-67.

10. Sarilita E, Soames R. Morphology of the Hard palate: a study of dry skulls and review of the literature. Rev Arg de Anat Clin 2015;7:34-43.

11. Ikuta CR, Cardoso CL, Ferreira-Junior O, et al. Position of the greater palatine foramen: an anatomical study through cone beam computed tomography images. Surg Radiol Anat 2013;35:837-42.

12. Beetge MM, Todorovic VS, Oettlé A, et al. A micro-CT study of the greater palatine foramen in human skulls. J Oral Sci 2018;60:51-6.

13. Benninger B, Andrews K, Carter W. Clinical measurements of hard palate and implications for subepithelial connective tissue grafts with suggestions for palatal nomenclature. J Oral Maxillofac Surg 2012;70:149-53.

14. Yu SK, Lee MH, Park BS, et al. Topographical relationship of the greater palatine artery and the palatal *spine*. Significance for periodontal surgery. J Clin Periodontol 2014;41:908-13.

15. Klosek SK, Rungruang T. Anatomical study of the greater palatine artery and related structures of the palatal vault: considerations for palate as the subepithelial connective tissue graft donor site. Surg Radiol Anat 2009;31:245-50.

16. Tavelli L, Barootchi S, Ravidà A, et al. What is the safety zone for palatal soft tissue graft harvesting based on the locations of the greater palatine artery and foramen? A systematic review. J Oral Maxillofac Surg 2019;77:271.e1-9.

17. Kim DH, Won SY, Bae JH, et al. Topography of the greater palatine artery and the palatal vault for various types of periodontal plastic surgery. Clin Anat 2014;27:578-84.

18. Reiser GM, Bruno JF, Mahan PE, Larkin LH. The subepithelial connective tissue graft palatal donor site: anatomic considerations for surgeons. Int J Periodontics Restorative Dent 1996;16:130-7.

19. Fu JH, Hasso DG, Yeh CY, et al. The accuracy of identifying the greater palatine neurovascular bundle: a cadaver study. J Periodontol 2011;82:1000-6.

20. Yilmaz HG, Ayali A. Evaluation of the neurovascular bundle position at the palate with cone beam computed tomography: an observational study. Head Face Med 2015;11:39.

21. Tucunduva MJ, Tucunduva-Neto R, Saieg M, et al. Vascular mapping of the face: B-mode and doppler ultrasonography study. Med Oral Patol Oral Cir Bucal 2016;21:e135-41.

22. D'haese J, Van De Velde T, Komiyama A, et al. Accuracy and complications using computer-designed stereolithographic surgical guides for oral rehabilitation by means of dental implants: a review of the literature. Clin Implant Dent Relat Res 2012;14:321-35.

23. Miwa Y, Asaumi R, Kawai T, et al. Morphological observation and CBCT of the bony canal structure of the groove and the location of blood vessels and nerves in the palatine of elderly human cadavers. Surg Radiol Anat 2018;40:199-206.

24. Landis JR, Koch GG. The measurement of observer agreement for categorical data. Biometrics 1977;33:159-74.

25. Koo TK, Li MY. A guideline of selecting and reporting intraclass correlation coefficients for reliability research. J Chiropr Med 2016;15:155-63.

26. Lee SP, Paik KS, Kim MK. Variations of the prominences of the bony palate and their relationship to complete dentures in Korean skulls. Clin Anat 2001;14:324-9.

27. Jeyaseelan N, Gupta M. Canals for the greater palatine nerve and vessels in the hard palate. J Anat 1988;156:231-3.

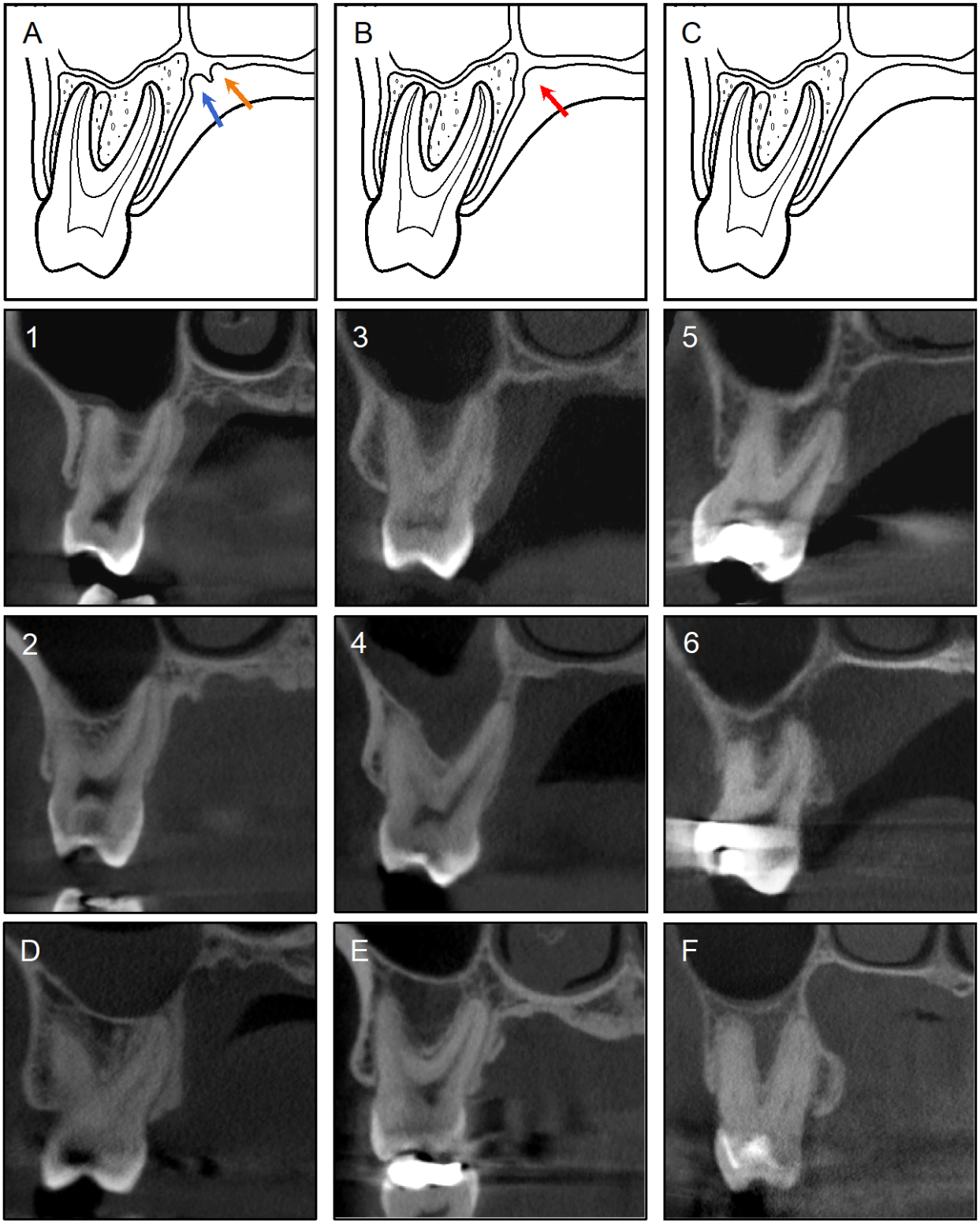

FIGURE 1 – CBCT Coronal Section Palatal Transition Morphology (PTM) Classification
Illustrations of (A) *Spine*, with medial (orange arrow) and lateral (blue arrow) grooves; (B) *Bridge*, with single groove (red arrow); and (C) *Smooth* PTM Types. Prototypical CBCT examples of (1-2) *Spine*, (3-4) *Bridge*, and (5-6) *Smooth* PTM classifications. Anatomical variations of (D) *Spine*, (E) *Bridge*, and (F) *Smooth* PTM.

Back

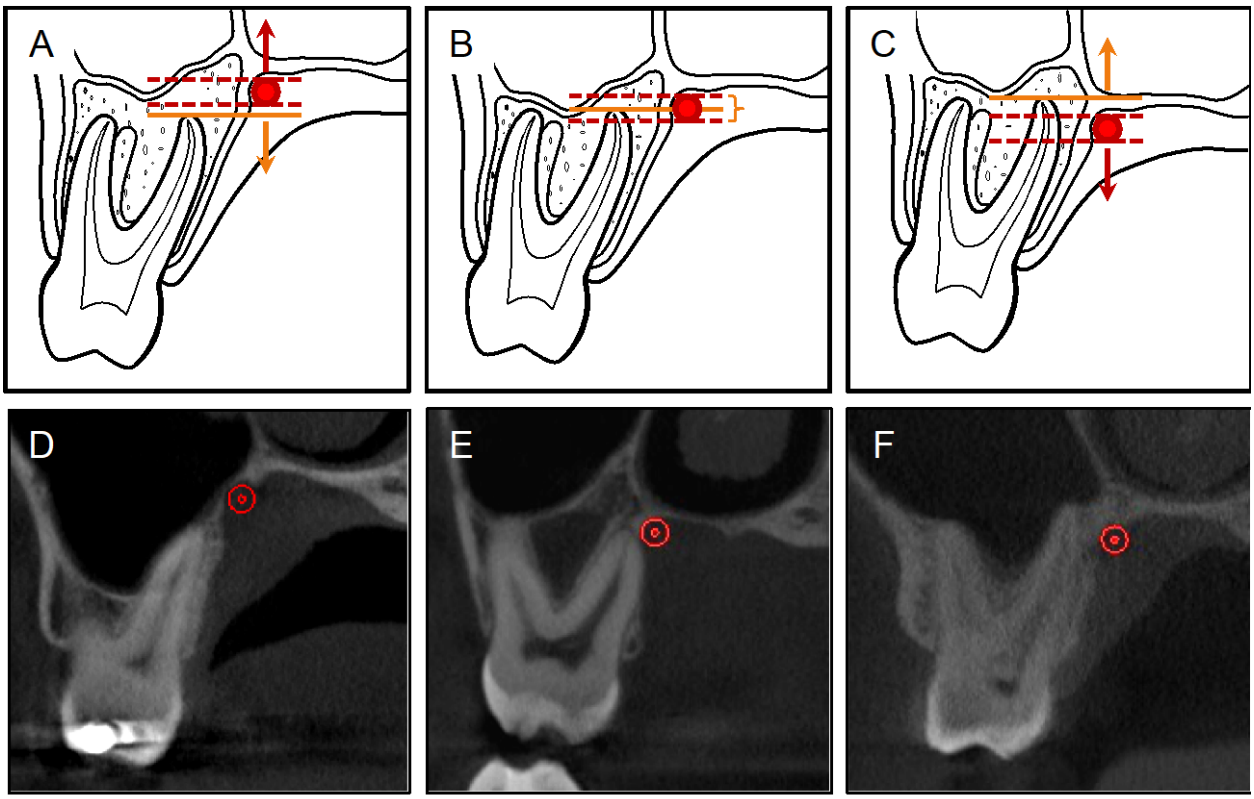

FIGURE 2 – Targeted Endodontic Microsurgery (TEMS) Greater Palatine Artery (GPA) Classification
Vertical GPA positions in relation to maxillary molar palatal root apices were classified as (A) *superior*, if the GPA diameter (red) was superior to a horizontal line (orange) drawn parallel to the hard palate and tangential to the the palatal root apex; (B) *adjacent*, if the root apex line was within the GPA diameter; or (C) *inferior*, if the GPA diameter was inferior to the root apex line. CBCT examples demonstrate (D) *superior*, (E) *adjacent*, or (F) *inferior* classifications. *Undefined* classifications were assigned when GPA position could not be reliably determined.

Back

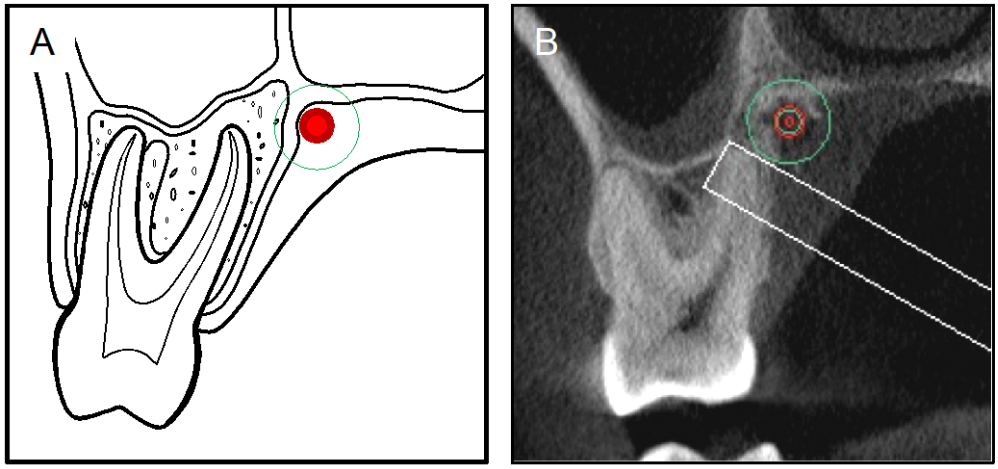

FIGURE 3 – (A) Illustration of the projected greater palatine artery (GPA) position and diameter (red), with a 2 mm safety margin (green) for maxillary molars. (B) CBCT example with trephine cross-section added for demonstration of palatal-approach Targeted Endodontic Microsurgery (TEMS) concept.

Back

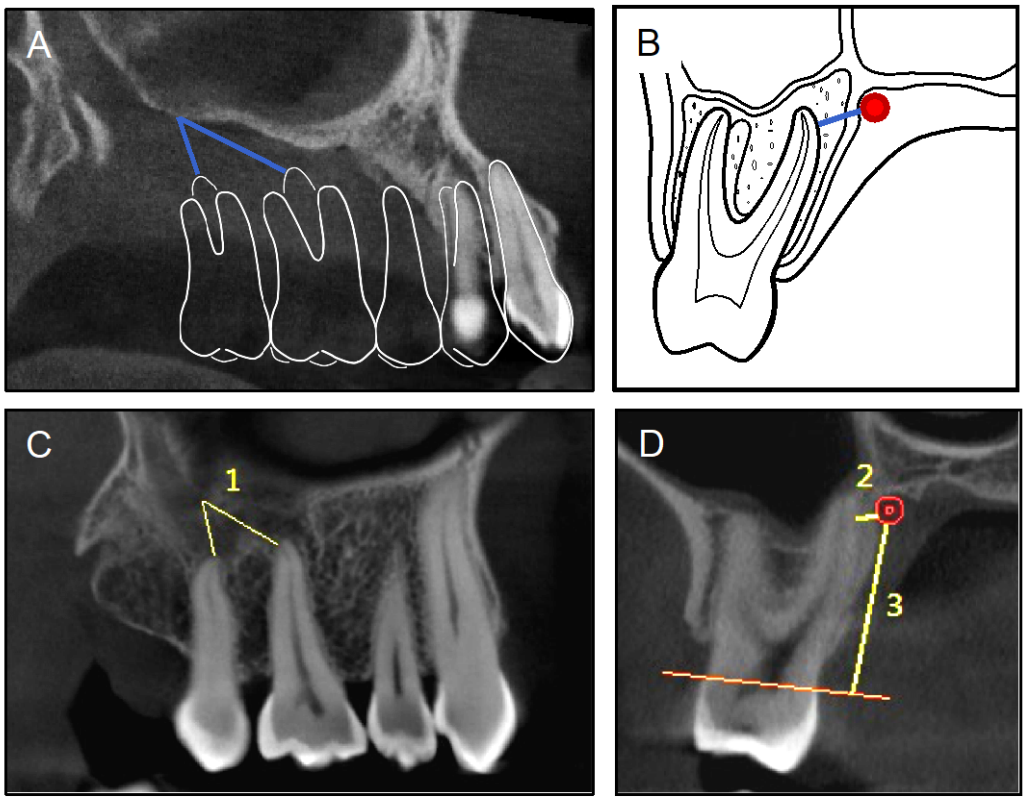

FIGURE 4 – (A) Illustrations of the shortest measured distances (blue lines) from the maxillary molar palatal roots to the closest border of the greater palatine foramen, and (B) the closest aspect of the greater palatine artery. (C) and (D) CBCT examples of the shortest distances (yellow lines) from the maxillary molar palatal roots to (C-1) the closest border of the greater palatine foramen, (D-2) the closest aspect of the greater palatine artery, and (D-3) the maxillary molar cemento-enamel junction to the inferior aspect of the greater palatine artery.

Back

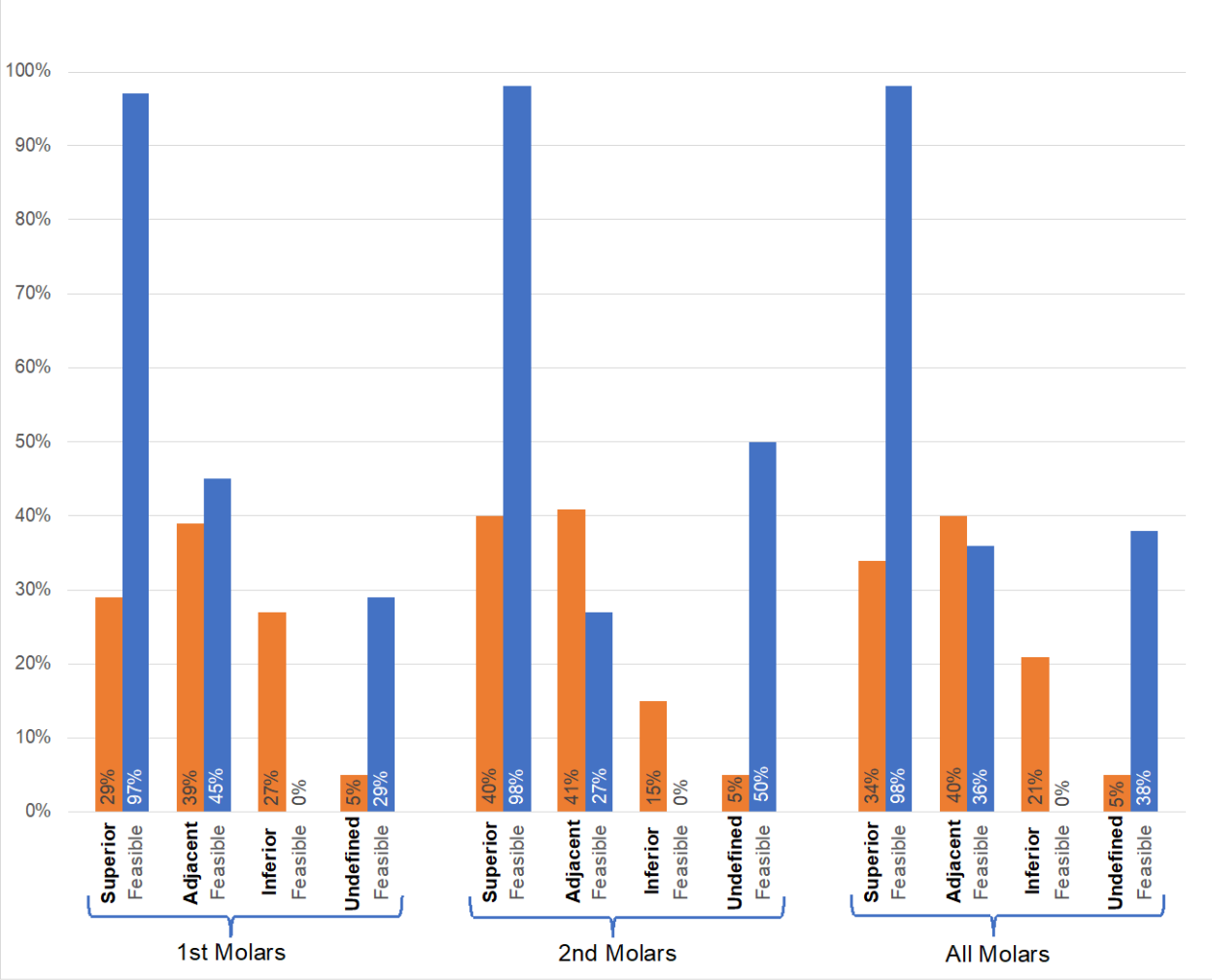

FIGURE 5 – Targeted Endodontic Microsurgery (TEMS) Classifications and Feasibility
Orange columns represent percentages of greater palatine arteries (GPA) classified as superior, adjacent, inferior, or undefined in relation to first molar (*N* = 126), second molar (*N* = 124), and combined molars' (*N* = 250) palatal root apices. Blue columns represent the percentage of TEMS-feasible molars in the orange classification column at their left. TEMS was deemed feasible for 97-98% of superior classifications, 27-45% of adjacent classifications, and no inferior classifications. Undefined classifications were deemed feasible in 29-50% of cases where evaluators agreed that, although the precise GPA location could not be determined, all possible locations were superior to the palatal root apices.

Back

TABLE 1 – Shortest Distances (mm) from Maxillary Molar Palatal Roots or Cemento-enamel Junctions (CEJ) to the Greater Palatine Foramen (GPF) or Greater Palatine Artery (GPA)

Measurement	1st Molars				2nd Molars				*p* Value	All Molars			
	N	Mean	SD	Range	*N*	Mean	SD	Range		*N*	Mean	SD	Range
Root–GPF	126	11.13	2.68	5.30 - 18.46	124	4.94	2.55	0.25 - 12.25	**< 0.0001**	250	8.06	4.06	0.25 - 18.46
Root--GPA	126	2.37	1.46	0.18 - 8.13	124	2.53	1.77	0.29 - 7.90	0.45	250	2.45	1.62	0.18 - 8.13
CEJ--GPA	126	12.86	2.29	7.30 - 18.44	124	14.05	2.52	7.08 - 19.88	**0.0001**	250	13.45	2.47	7.08 - 19.88

TABLE 2 – Shortest Distances (mm) from Maxillary Molar Palatal Roots or Cemento-enamel Junctions (CEJ) to the Greater Palatine Foramen (GPF) or Greater Palatine Artery (GPA) for Females and Males

Measurement	Female				Male				*p* Value
	N	Mean	SD	Range	*N*	Mean	SD	Range	
Root--GPF	122	7.95	3.84	0.60 - 14.93	128	8.17	4.27	0.25 - 18.46	0.66
Root--GPA	122	2.51	1.50	0.18 - 7.90	128	2.39	1.72	0.25 - 8.13	0.57
CEJ--GPA	122	12.54	2.56	7.08 - 19.88	128	14.33	2.04	10.36 - 18.83	**< 0.0001**

TABLE 3 – Shortest Distances (mm) from Maxillary Molar Palatal Roots or Cemento-enamel Junctions (CEJ) to the Greater Palatine Foramen (GPF) or Greater Palatine Artery (GPA) for Right and Left Sides

Measurement	Right				Left				*p* Value
	N	Mean	SD	Range	*N*	Mean	SD	Range	
Root--GPF	115	7.85	3.91	0.60 - 17.46	135	8.24	4.19	0.25 - 18.46	0.45
Root--GPA	115	2.45	1.57	0.29 - 7.70	135	2.44	1.66	0.18 - 8.13	0.97
CEJ--GPA	115	13.50	2.45	7.08 - 18.83	135	13.42	2.50	8.10 - 19.88	0.80

Back